OPERATING A PHOTOMULTIPLIER AT LIQUID-HELIUM TEMPERATURE

Hans-Otto Meyer (meyer1@indiana.edu), Indiana University, November 2007

1. Summary

The performance of a Hamamatsu R7725-mod photomultiplier (PM), featuring a photocathode with a platinum underlayer, has been studied at cryogenic temperatures, down to 4 K. Its parameters are compared to those of a tube of the same model without a cathode underlayer. Measurements are carried out by observing the response of the PM to short, low-intensity light pulses. It is found that

- The quantum efficiency Q of the modified PM is affected only weakly by cooling. At liquid-helium temperature ($T_{\ell He}$) Q is still 90% of its value at room temperature (T_{room}). At T_{room}, the quantum efficiency of a modified PM is lower than that of a normal PM because of light absorption in the platinum layer, but a normal PM stops working below 150 K. I found that Q does not depend on the intensity of the light pulses, i.e., on the electron current emerging from the cathode (!).
- The gain G of the modified PM at $T_{\ell He}$ is about ⅔ of its value at T_{room}, a loss of gain that may be recovered by raising the tube voltage by about 150 V. When cooling a normal PM from T_{room} to 170 K, an increase in gain by about 30% was observed. A similar increase was not found for the modified PM, suggesting that the two tubes are different in more ways that just the platinum underlayer.
- Starting at T_{room}, the dark rate n_d decreases with temperature in a way that is consistent with thermionic emission, reaches a minimum near 200 K, then rises monotonically until $T_{\ell He}$ is reached. Dark events at low temperature originate at the cathode, and dark events are not independent of each other (bursts?). I have not found any information on the mechanism of their generation.
- Afterpulses are caused by ionization of the residual gas in the PM. The number of afterpulses N_a that follow a light pulse is thus proportional to the electron current, or to the number of photoelectrons emitted from the photocathode by that pulse. For a one-photoelectron event, N_a is typically about 0.01. From T_{room} to $T_{\ell He}$ N_a decreases by about 10%. Increasing the tube voltage, increases N_a, presumably because of the change in the ionization cross section. Most afterpulses occur within 4 μs of the primary event. Increasing the tube voltage shifts their time distribution towards smaller times.
- Helium poisoning of the PM has been studied by storing the tube for 12 hours at $T_{\ell He}$ in a dense He gas. The test container was then evacuated again. After warm up, the afterpulse spectrum showed no change. Thus, I have found no evidence against exposing a PM to helium at $T_{\ell He}$.

These findings are discussed in detail in sect.2. The technical aspects of the experiment are described in sect.3. References to related work are given in sect. 4.

2. Measurements and Results

2.1. Photomultipliers

The Hamamatsu R7725 is a 5 cm diameter PM with a K-Cs-Sb (bialkali) photocathode. The dynodes are Cu-BeO-Cs. The maximum quantum efficiency (at 420 nm) is quoted as $Q_{nominal} = 0.26$. I had five tubes at my disposition, two normal ones (serial #3378 and #3379), and three with a platinum underlayer (serial #3692, #3693 and #3697). At T_{room} and $U_{PM} = 1750$V the gains of the five tubes vary from $4 \cdot 10^7$ to $9 \cdot 10^7$. I have measured that the presence of a Pt layer lowers the quantum efficiency by a factor 0.78.

Only two of these tubes (#3378 and #3692) are actually used in the cold test described here.

2.2. Apparatus

The photomultiplier (PM) under test is housed in an evacuated cylindrical container, which is inserted into the well of a bucket dewar. Thus, the PM is cooled by radiation. This is necessary in order to slow the cooling rate. Fig.1 shows an example of the temperature T of the surface of the tube near the cathode versus time for a test run. First, the liquid nitrogen (ℓN_2) jacket of the dewar is filled (point A). Initially, the cooling rate is about 30 K/h. When T starts to approach an equilibrium, the well is also filled with ℓN_2 (point B), and eventually, the ℓN_2 in the well is replaced by ℓHe (point C). Cooling may be accelerated by temporarily admitting He gas to the test container.

The temperature is measured at the wall of the container, at the rear end of the PM, and on the glass surface near the photocathode. Temperature values T, as quoted in the remainder of this document, refer to the temperature of the cathode. There are indications that the temperature of the interior of the PM differs substantially from T (see sect. 2.7). In equilibrium at $T_{\ell He}$, I estimate that temperature of the dynode structure is between 10 and 15 K.

Except for a 6.4 mm diameter hole in the center of the cathode, the PM is covered with black tape. Thus only 1.6% of the photocathode is in use. Blue light pulses ($\lambda = 467$ nm) of 10 ns width and variable amplitude are carried by fiber optics to a splitter in front of the photocathode. The splitter sends about half the light diffusely in the direction of the photocathode, while the remainder of the light returns via optical fiber to a detector at room temperature that continuously monitors the intensity of the light pulses. Pulses are generated at a rate of 3.5 kHz.

The anode pulses are amplified (optional) and sent to a charge-integrating ADC and a discriminator. The light pulse trigger also starts a TDC, which registers the time of occurrence of up to 16 anode pulses (including the initial event) that follow a given light pulse.

More details about the apparatus can be found in sect. 3.

2.3. Quantum efficiency Q

A typical ADC spectrum is shown in fig.2. As can be seen, the one-photoelectron (1pe) peak is distinct from the 2pe peak, and well separated from the pedestal, which contains events without PM response. The probability to find k pe's is given by a Poisson distribution $p(k,\kappa)$, where κ is the average number of pe's. The value of κ may be determined by fitting the spectrum with a series of Gaussians, or more simply, by

counting the number of events in the pedestal. Except for an overall constant, the quantum efficiency Q is obtained by dividing κ by the light pulse intensity (measured by the monitor, see sect.3.3). An overall constant is chosen such that at room temperature Q = 0.25 for a normal PM, and Q = 0.20 for a PM with a Pt underlayer.

Cooling from T_{room} to $T_{\ell He}$ lowers Q of the modified PM by about 10% (blue and red symbols in fig.3). Thus, the modified PM is not much affected by cooling. The effect of the Pt underlayer is obvious when comparing this to the behavior of a normal PM (green symbols in fig.3), which stops working below about 170 K.

The green data point in fig.3 near T = 160 K, Q = 0.1 is actually a superposition of four measurements taken with light intensities varying by about a factor of 10. Apparently, Q does *not* depend on the intensity of the light pulses, or in other words, on the electron current emerging from the cathode. This is puzzling since it is believed that the failure of a normal PM is due to the exponential rise in cathode resistivity with falling T, leading to a charge buildup on the cathode, which must depend on the electron current.

One would expect that Q also depends on the tube voltage U_{PM}, however the effect is too small to be seen in this experiment.

2.4. Gain *G*

The gain G is determined by measuring the charge at the anode for a 1pe (or 2pe) event. The charge measurement is based on the peak position in the spectrum (minus the pedestal) and the nominal calibration of the ADC (0.25 pC per channel).

Cooling from T_{room} to $T_{\ell He}$ lowers G of the modified PM by a factor of 0.67 (see fig.4a). The knee with the sharp drop at 77 K is due to the fact that the dynode temperature is lagging behind the measured cathode temperature T. This effect will be discussed in sect. 2.7. I assume that if G were plotted against the *actual* dynode temperature (which is unknown), the data would line up along the red dashed curve. It is worth noting that a similar knee was observed in a recent study of a PM at 29 K [NIK07].

The same measurement for a normal PM is shown in fig. 4b. In this case, the gain G is found to *increase* by about 30% between T_{room} and about 170 K. Such an increase is not observed in the modified PM. This would mean that there other differences between the normal and modified tubes than just the Pt underlayer.

The gain G as a function of the tube voltage U_{PM} is shown in fig.5 measured at T_{room} and $T_{\ell He}$. The solid lines represent the function

$$G = const. \cdot \left(U_{PM}\right)^{\alpha \cdot N} \quad , \tag{1}$$

where N = 12 is the number of stages and α = 0.62 ± 0.02, independent of T. It can be seen that an increase of U_{PM} by 150 V is sufficient to recover the loss of gain due to cooling.

2.5. Dark rate n_d

The dark rate is the rate of events observed with no light on the PM. A dark event is defined by the discriminator threshold, which is set at about 20% of the amplitude of a 1pe response (in other words the definition is robust against changes in gain). The value of n_d may be determined from the uniform population of the TDC spectrum, or by simply counting the discriminator outputs for a certain amount of time. The latter method is more accurate, but the two methods agree.

The dark rate n_d at T_{room} varies widely from tube to tube. For the normal tubes (#3378, #3379) n_d is 3000 Hz and 900 Hz, respectively, while for the modified tubes (#3692, #3692, #3692) n_d is 200 Hz, 400 Hz and 75 Hz, respectively.

Fig. 6 shows the dark rate as a function of temperature for the tested, modified PM (#3692). Between T_{room} and about 250 K, n_d decreases in a way that is consistent with thermionic emission. This is illustrated by the green line which represents Richardson's law

$$n_{d,therm} = const. \cdot T^2 \cdot e^{-\frac{W}{kT}} \quad , \tag{2}$$

where W = 0.43 eV is the work function (adjusted to fit the slope). After reaching a minimum near 200 K, n_d increases monotonically all the way to $T_{\ell He}$.

These non-thermionic dark events are not independent of each other. Most likely, they occur in bursts. This is demonstrated by taking a large number of 5-second measurements of the dark rate at 6 K (see fig.7). The data are shown with their statistical uncertainties; their actual standard deviation is about 5 times larger.

The dark rate as a function of tube voltage U_{PM} is shown in fig.8 for three temperatures. At T_{room}, the voltage dependence is consistent with the Schottky effect, i.e., it is proportional to $\exp\left(b\sqrt{U_{PM}}\right)$ (solid blue line). However, this statement is not very meaningful, since it is impossible to estimate the expected value of the constant b without detailed knowledge of the field distribution inside the tube.

At the lower temperatures, n_d depends only weakly or not at all on U_{PM}. This seems to rule out field emission as a possible dark-rate generating mechanism. It is interesting to note that n_d as a function of T (fig.6) does not exhibit the pronounced knee near 77 K that is seen in the case of the gain G as a function of T (fig.4). This indicates, that the dark events originate at the place where T is actually measured, i.e., at the *photocathode*.

The non-thermionic dark rate has been studied and discussed previously [ROD63, GAD65], and it has been known for 40 years that their rate is independent of U_{PM}, that the events originate at the cathode, and that they are not Poisson-distributed in time. As far as I know, none of this is really understood. My results are consistent with those of a recent study of a PM at 29 K [NIK07].

2.6. Afterpulses N_a

Afterpulses occur due to the ionization of residual gas molecules by the electrons from some 'primary' event. The number of afterpulses that follow an event is thus proportional to the electron current, or to the number of electrons emitted from the photocathode, or the light pulse intensity. For simplicity, all measurements of N_a quoted here are normalized to correspond to a 1-photoelectron event ($\kappa = 1$). For the measurement of N_a I am using an LRS 2277 TDC that registers the time of occurrence of multiple discriminator pulses, relative to the trigger of the light pulse.

When cooling the PM, N_a decreases only slightly (fig.9). This indicates that the gas density inside the tube at $T_{\ell He}$ is more or less the same as at T_{room}. On the other hand, N_a depends strongly on the tube voltage (fig.10), presumably because of the ionization cross section increases with increasing average electron energy.

Fig. 11 shows the time distribution of the afterpulses as a function of the tube voltage U_{PM}. Most afterpulses occur within 4 μs. Increasing the tube voltage shifts the distribution towards smaller times.

2.7. Dynode cooling and helium poisoning

From fig.4 one sees that during initial cooling towards $T_{\ell N2}$ the gain G changes slowly, but keeps on changing after T = 77 K has been reached. This suggests that the actual dynode temperature is lagging behind the measured T against which the data in fig.4 are plotted. Fig. 12 shows the relative gain for all measurements between 75 K and 79 K *as a function of time*. The measured time dependence is well explained by an exponential decrease with a time constant $\tau \sim 1.8$ days (solid line in fig.12). This long equilibration time (of the dynode temperature) is probably affected by the fact that the dynodes are not just well-insulated, but also heated via conduction along the attached wires.

It is well known that exposure of a PM to He gas destroys the PM, because He diffuses easily through the glass, and raises the residual gas pressure inside the tube. However, at cryogenic temperatures the diffusion constant [ROG54], which depends exponentially on $1/T$, is negligible, and no helium poisoning of the PM is expected under this condition. To test this, I have exposed the tube at 8 K to helium gas for 12 hours. The gas density was estimated to several bars equivalent at room temperature. Fig. 13 shows the afterpulse time distribution before the experiment and after several days after warm up. It is obvious that there is no significant change, and thus I have found no evidence against operating the PM in a cold He environment from this short-term (compared to the lifetime of nEDM) test.

3. Technical details

3.1. Overview

The test container consists of a 12” long, 3” O.D. stainless steel tube, welded shut at one end and closed by a conflat flange [DUN-F] with copper seal at the other end. This assembly is hanging from the ‘top flange’ by three 43” long, 0.25 diameter G10 rods (see fig.14). A 0.75” diameter corrugated, flexible, stainless steel hose [MDC-H] connects the cold test container to the top flange, which is at room temperature and closes the well volume of the dewar. Five radiation baffles are made from Styrofoam, covered with kitchen foil, and are held in place by paper clips.

Inside the test container, the PM under test (#1 in fig.15) rests on two G10 rods. The photocathode is covered with a black aluminum diaphragm with a 0.25” hole in the center (thus only 1.6% of the photocathode is in use), and the whole PM is wrapped with black paper tape (3M #235). The light source (sect. 3.3) is 3.5 cm in front of this hole. Temperature sensors [LSH-T] are connected to the inside of the container wall, the rear end of the PM and a point near the photocathode (#6-8). Temperature values are read out by a 218E controller [LSH-T] and logged every 2 minutes during the entire experiment.

The test container, connecting tube and manifold are evacuated by a Pfeiffer TMU071 turbo pump (on loan from Los Alamos), backed by a 1.5 l/min fore pump, purchased for this purpose [LES-P]. The only pressure measurement is by a borrowed thermocouple gauge. The pumping manifold includes a relief valve to vent condensed gases during warm-up. The vacuum feedthrough of all wire connections is achieved by multi-pin

Amphenol connectors, glued with Stycast into the feed-through box (fig.16). A sealing BNC connector is used for the signal cable.

3.2. PM base and connections

The photomultipliers used have been listed in sect 2.1. The base circuit used (fig.17), with minor modifications, follows the recommendation by Hamamatsu. Resistors and capacitors used are listed in fig.17; these components have been tested in ℓN_2 for their cryogenic performance prior to use. In order to avoid the associated heat load, the voltage divider is located at room temperature, outside the vacuum, with connections to the individual dynodes made by a specially constructed, 16-lead ribbon cable. This ribbon cable (fig.18) consists of four quad phosphor-bronze cables [LSH-C], embedded in insulating lacquer, sandwiched between layers of Kapton. With this cable, the PM has been biased up to 2000 V. The signal connection is made with a stainless steel coax cable [LSH-C].

3.3. Light source

The light source is a surface-mount LITEON LTST-C150TBKT blue LED, which emits at a wavelength of 470 nm with a FWHM of 50 nm. The LED is driven by the circuit shown in fig. 19. The switching elements ($Q_{1,2}$) are two BSS138 DMOS field-effect transistors. The assembled circuit is also shown in fig.19. The light intensity depends (non-linearly) on the DC voltage supplied to the capacitor C_1. This parameter was used to vary the electron current from the cathode, while the pulse rate was fixed at 3.5 kHz throughout the experiment.

The light is transported by a 0.5 mm diameter, step-index, plastic optical fiber (#3 in fig.15) to a splitter 3.5 cm in front of the photocathode. The splitter sends about half the light diffusely towards the PM, and the other half back out to a monitor photomultiplier. Thus, the monitor measures the return light. The splitter is made from a small block of acrylic with sanded surfaces, with a 0.5 mm hole drilled through (fig.20). Rough-cut fiber ends are inserted into the hole and secured in place with 5-minute epoxy. In effect, the splitter is a leaky fiber splice.

During cooling, it was observed that the monitor light decreases by some 10% between T_{room} and $T_{\ell He}$ (fig.21). This could be either because the fiber transmission depends on temperature, or because the splitting fraction changes. This question has been decided by cooling a 5 m spool of optical fiber with ℓN_2, which actually slightly (by 1-2%) *increased* its transmission. Thus, a temperature-dependent splitting fraction is responsible for the 10% change, and a (small) correction is applied when deducing the light pulse intensity from the monitor signal.

3.4. Cryogenics and thermal performance

When using cryo liquids for cooling, the system temperature changes continuously, except when at the corresponding boiling temperatures. To keep the cooling rate low, the PM has been cooled by radiation. The largest cooling rate (about 30 K/hour) occurs at the beginning of the cooling procedure. This cooling rate has had no ill effect on either of the two tested PMs. To increase the emissivity, the inside of the test container has been coated with black paint, and the PM is wrapped in black paper tape (3M#235). Paper tape is used, since the usual black electrical tape fractures when cooled!). Cooling by radiation is illustrated in fig.22. The temperature of the PM as a function of time when approaching

ℓN_2 equilibrium is shown by blue dots. The red, solid curve is calculated assuming an emissivity of 0.5 for both, PM and container inside wall.

Near $T_{\ell He}$ radiation cooling is slow. In thermal equilibrium, the heat flow to the PM is compensated when the PM is at about 10 K. The heat flow takes place through the wires, which are touching the tube leading to the test container, and are thus partly heat sunk. All phosphor bronze wires leading to the PM and the signal cable together would carry about 1.5 mW if between 300 K and 4 K. However, the wires are partly heat-sunk by touching the long, flexible tube between the top flange and the test container.

3.5. Electronics and data acquisition

The anode signal is either amplified by an LRS 621 BL (NIM electronics) or sent directly to a 4300B charge-integrating FERA CAMAC ADC. Timing data are acquired with a LRS 2277 TDC, which is started with every pulse trigger, and stopped by the discriminated anode signal. Up to 16 stop signals are recorded within a 16 μs interval after the start (different configuration are possible). A Wiener CCUSB CAMAC crate controller is used. The data acquisition software is the standard IUCF code XSYS. Offline analysis has been carried out, using Mathcad and Excel.

4. Context

It has been 60 years since, for the first time, a photomultiplier has been studied at liquid nitrogen temperature [ENG47]. Cooling photomultipliers, originally aimed at noise reduction, has recently become of interest in exploiting the scintillating properties of liquid noble gases. For such use, tubes with bialkali photocathodes are preferred because of their low dark noise.

It was realized relatively early that bialkali tubes, when cooled, fail abruptly at a temperature near 150 K (e.g., [ICH93]). This was attributed to the rapidly increasing (with falling temperature) resistivity of the cathode material. Electrons emitted from the cathode would then cause a build-up of an opposing potential. A quantitative model to explain the measured pulse height versus temperature met with some success [ARA98].

At least two companies, Electron Tubes Ltd. and Hamamatsu Photonics, are now producing tubes where the resistivity problem is addressed by underlaying the cathode with a thin metal layer (e.g., platinum). A number of studies (e.g., [ANK06, PRA06]) have shown that such tubes can be operated at liquid nitrogen temperature. More recently, a group at Yale has cooled a photomultiplier to 29 K [NIK07]. While the bottom line for the last three references is the same as that of the present report, namely that platinum-modified PMs can be operated at cryogenic temperatures, there are clear differences between the results of the various studies, presumably because of differences in geometry and dynode materials for the various tube types.

In the present study a single PM type has been cooled to liquid helium temperature. This was motivated by a planned measurement of the electric dipole moment of the neutron (http://p25ext.lanl.gov/edm/edm.html). This experiment features a reaction volume at a temperature below 1 K where the experimental signal consists of scintillation in liquid helium. Being able to operate the PM at liquid-helium temperature, increases the light collection efficiency significantly.

5. References

[ANK06] A. Ankowski et al., *Characterization of ETL 9357FLA photomultiplier tubes for cryogenic temperature applications*, Nucl. Instr. Meth A556, 146 (2006)

[ARA98] H.M. Araujo et al., *Study of bialkali photocathadodes below room temperature in the UV/VUV region*, IEEE Trns. Nucl. Sci. 45, 542 (1998)

[DUN-F] Duniway Corp., www.duniway.com. Conflat flanges, one with 3" ID, the other modified; F458-300N, F458-000

[ENG47] R.W. Engstroem, *Refrigerator for multiplier phototube*, Rev. Sci. Instr. 18, 587 (1947)

[GAD65] M Gadsden, *Some statistical properties of pulses from photomultipliers*, Appl. Opt. 4, 1446 (1965)

[ICH93] M. Ichige et al., *Operating characteristics of photomultipliers at low temperature*, Nucl. Instr. Meth. A327, 144 (1993)

[LSH-T] Lake Shore Cryotronics Inc., www.lakeshore.com. Silicon temperature sensor DT-470-SD-13, controller 218E,

[LES-P] Kurt Lesker, http://www.lesker.com. BOC Edwards rotary vane fore pump ED-A37122902, E2M1.5

[LSH-C] Lake Shore Cryotronics Inc., www.lakeshore.com. WQL-36-100, 100ft 36AWG quad lead ribbon wire, CC-SS-25 25ft stranded stainless coax cable

[NIK07] J.A. Nikkel et al., *Demonstration of photomultiplier tube operation at 29 K*, arXiv:astro-ph/0702202v1, 7 Feb 2007

[MDC-H] MDC Vacuum Prod., www.mdcvacuum.com. Flexible stainless steel hose, UB-FRLT-075-36; ¾" OD, 0.005" wall; 36" long, 4 pounds,

[PRA06] M. Prata et al., *Performance and behaviour of photomultiplier tubes at cryogenic temperature*, Nucl. Instr, Meth. A567, 222 (2006)

[ROG54] W.A. Rogers, R.S. Burtz and D. Alpert, *Diffusion coefficient, solubility, and permeability for helium in glass*, J. Appl. Phys. 25, 868 (1954)

[ROD63] J.P. Rodman and H.J. Smith, *Tests of photomultipliers for astronomical pulse-counting applications*, Appl. Opt. 2, 181 (1963)

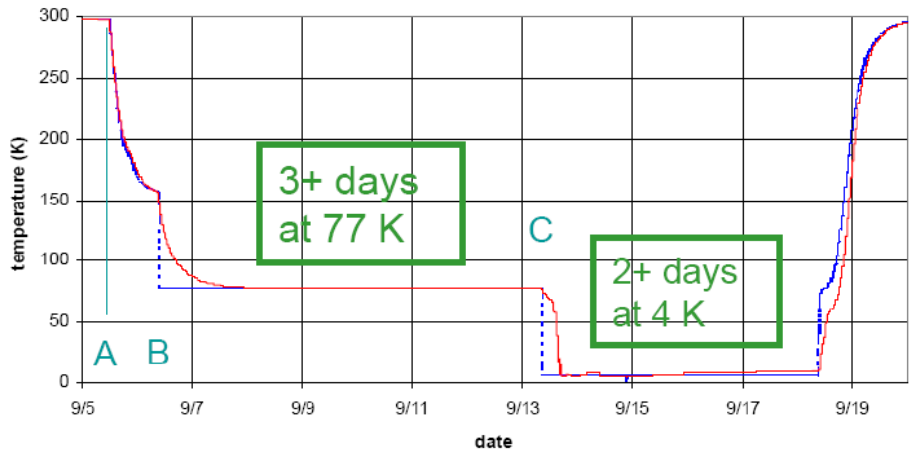

Fig.1: temperature history for the run with the modified ZK3692. The blue and red curves refer to the wall of the test container, and a point on the PM near the photocathode, respectively. The labels A and B mark the insertion of ℓN2 into the jacket and the well, respectively. At C, the ℓN2 in the well was removed and replaced by ℓHe.

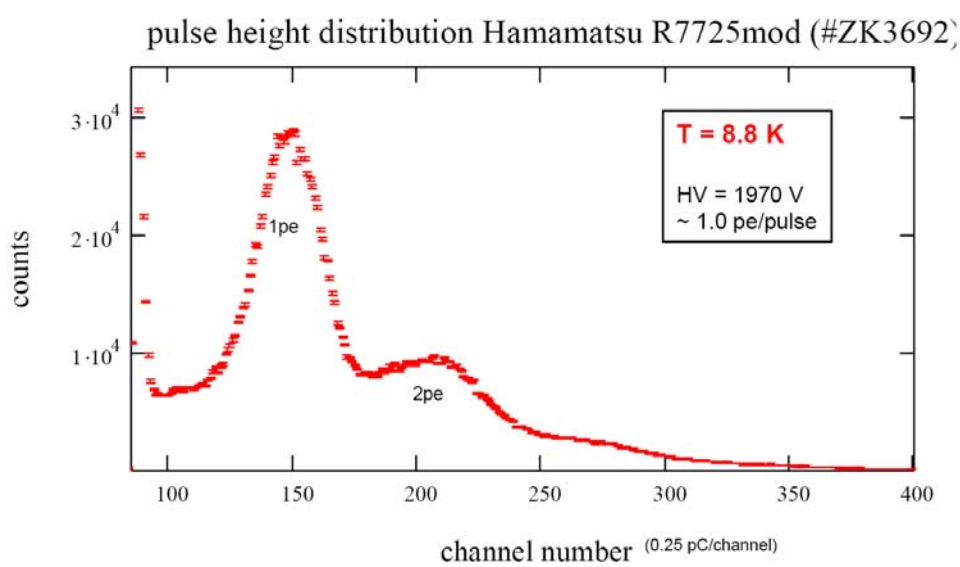

Fig.2: pulse height spectrum of the modified tube at $T = 8.8$ K. The average pulse corresponds to about 1 photoelectron.

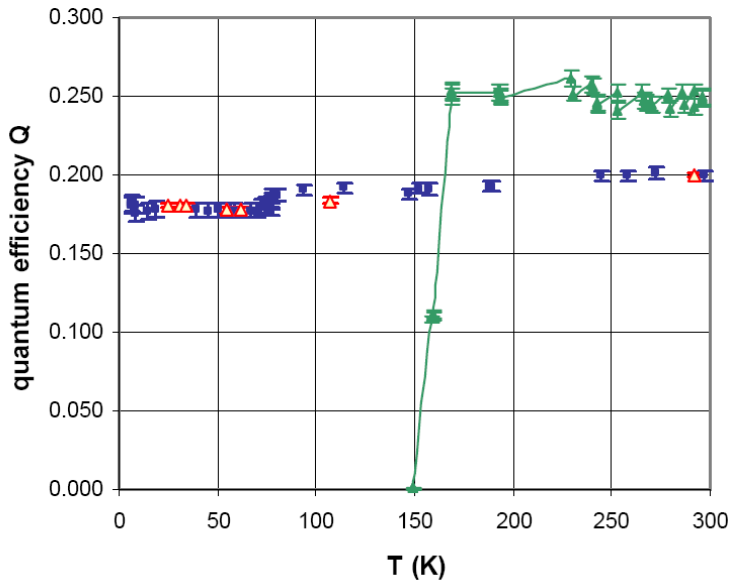

Fig.3: quantum efficiency versus temperature for a normal PM (green data), and for a modified tube (blue and red data, measured during cool-down and warm-up, respectively). The error bars take into account the arbitrariness in determining the average number of photoelectrons.

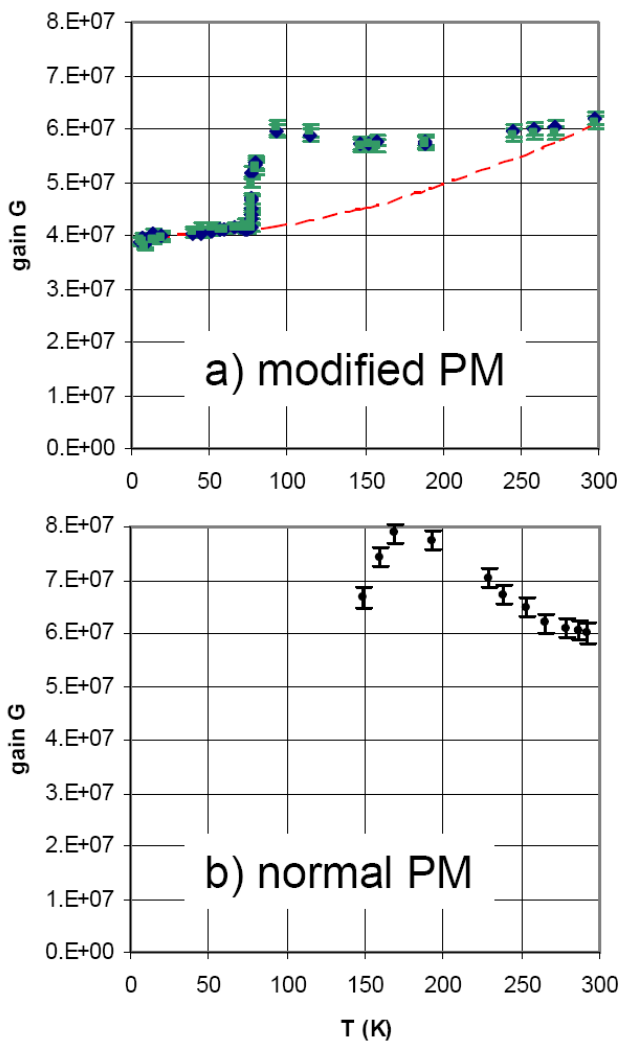

Fig.4: gain at U_{PM} = 1720 V versus temperature for a) a modified tube, and b) a normal tube. The knee in fig. 4a is due to the fact that the dynode temperature is lagging behind the measured cathode temperature *T*. The normal PM shown in fig. 4b, does not work below 150K (see also fig.3).

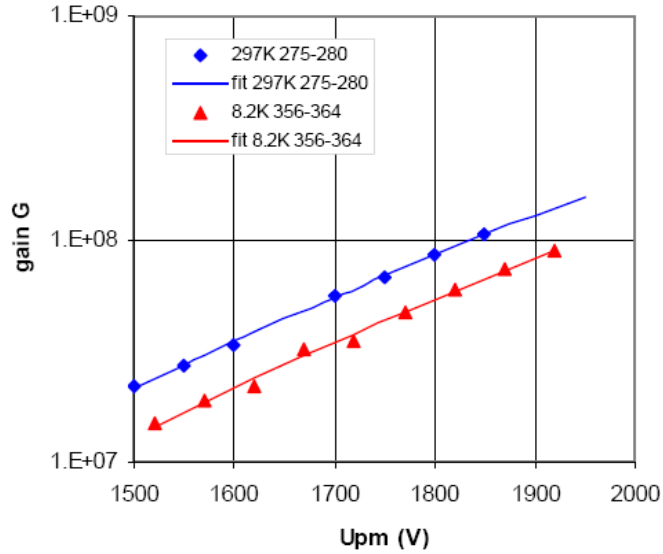

Fig.5: gain G vs U_{PM} of the modified PM (#3692) at T = 297 K and 8 K. The lines are fits with G proportional to U_{PM}^($N\alpha$), where the number of stages is N=12, and α = 0.62+/-0.02. It can be seen that to make up for the gain that is lost by cooling, an increase of U_{PM} by ~150V is needed

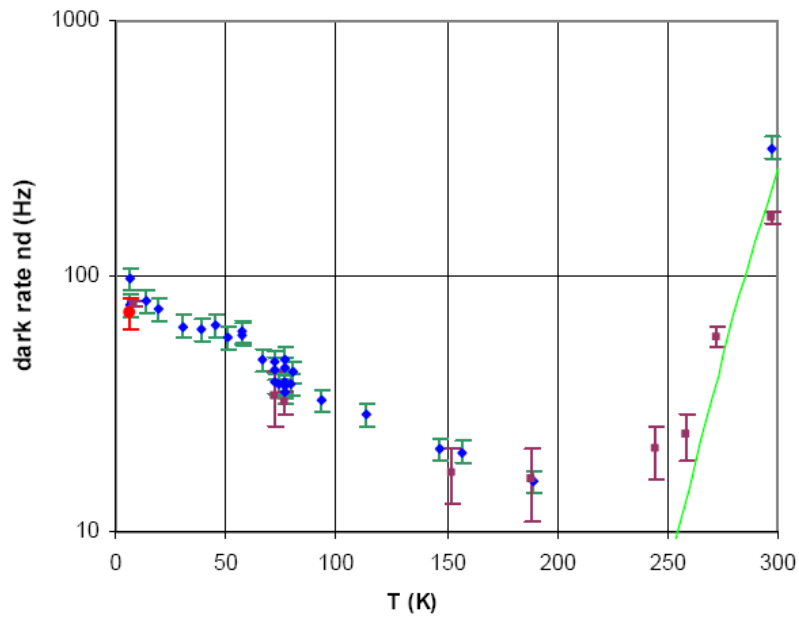

Fig.6: dark rate as a function of T for the modified PM (#3692). Different color data points represent different methods to evaluate the dark rate. The green curve is consistent with thermionic emission, assuming a work function of W=0.43 eV.

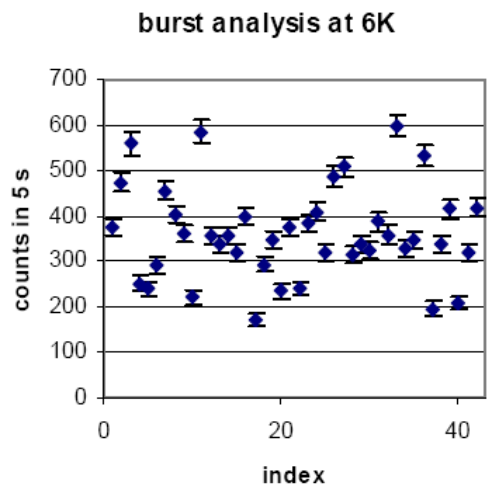

Fig.7: 42 measurements of the dark yield in 5 s at 8 K and U_{PM} = 1720V. The error bars correspond to the square root of the yield, as expected from Poisson statistics). This demonstrates that dark events are *not* independent in time. The average yield is 362, the deduced rms value of a single measurement is about 100, i.e., 5 times larger than the Poisson uncertainty.

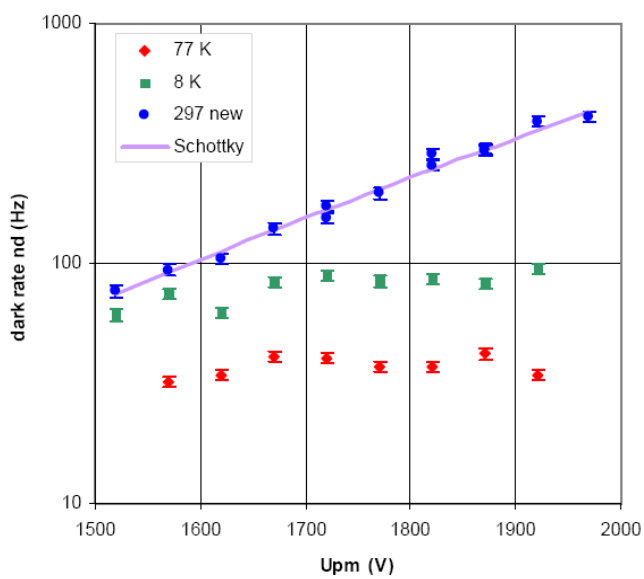

Fig.8: dark rate as a function of the tube voltage U_{PM}, measured at three different temperatures. The solid line is consistent with the the temperature dependence of the Schottky effect in thermal emission.

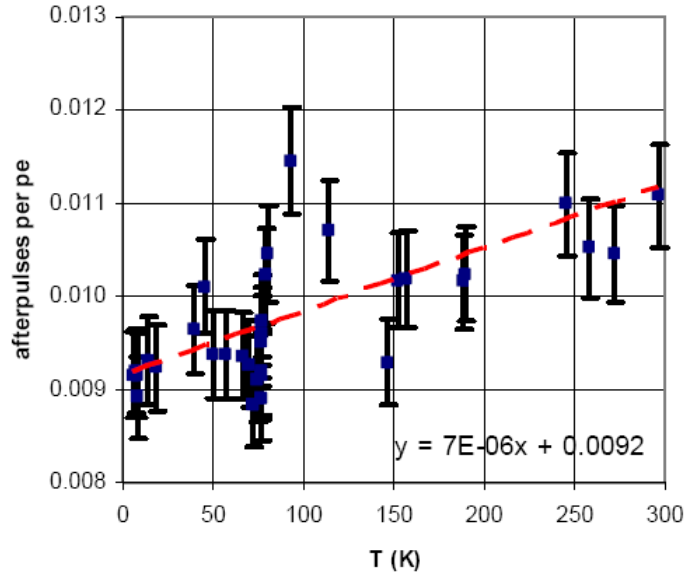

Fig.9: temperature dependence of the number of afterpulses following an event with 1 photo electron. The errors shown are statistical. The tube voltage U_{PM} was 1720 V.

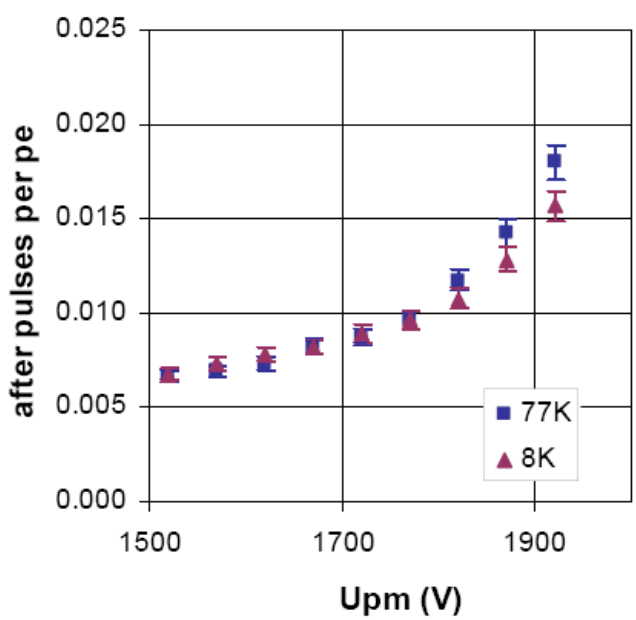

Fig.10: number of afterpulses following an event with 1 photo electron, as a function of the tube voltage U_{PM}, measured at two different temperatures. The errors shown are statistical.

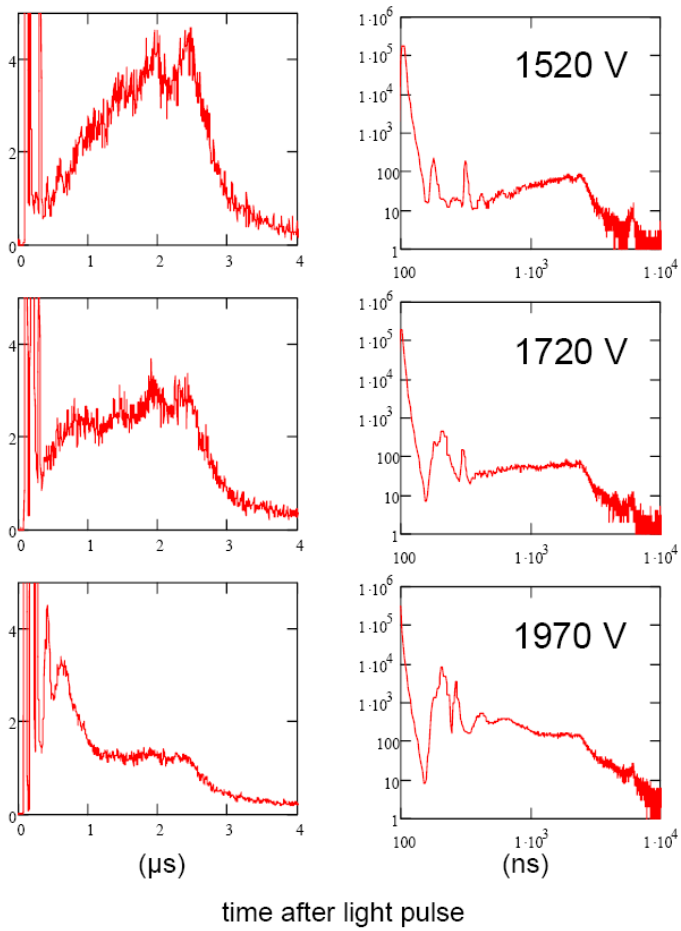

Fig.11: time distribution of afterpulses after a primary event with an average of 4 photo electrons. The data are taken at room temperature. Except for the axes (lin/log), the figs. on the left and the right are the same. The time distribution is affected by the tube voltage U_{PM} (indicated in the right column). The LED driving voltage was 20 V.

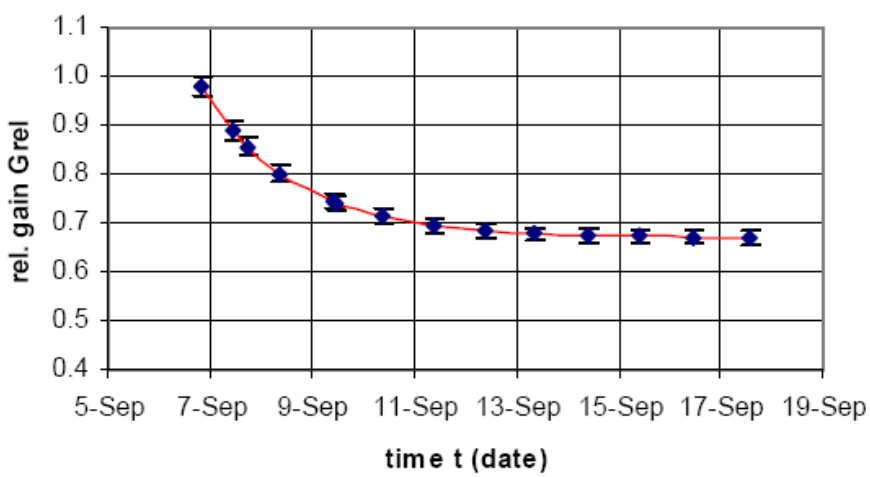

Fig.12: relative gain, measured near 77 K, versus time. The red line represents an exponential function with a decay constant of 1.8 days (!). This shows that the dynode temperature is lagging behind and thus explains the knee in the measured gain versus T (fig.4a).

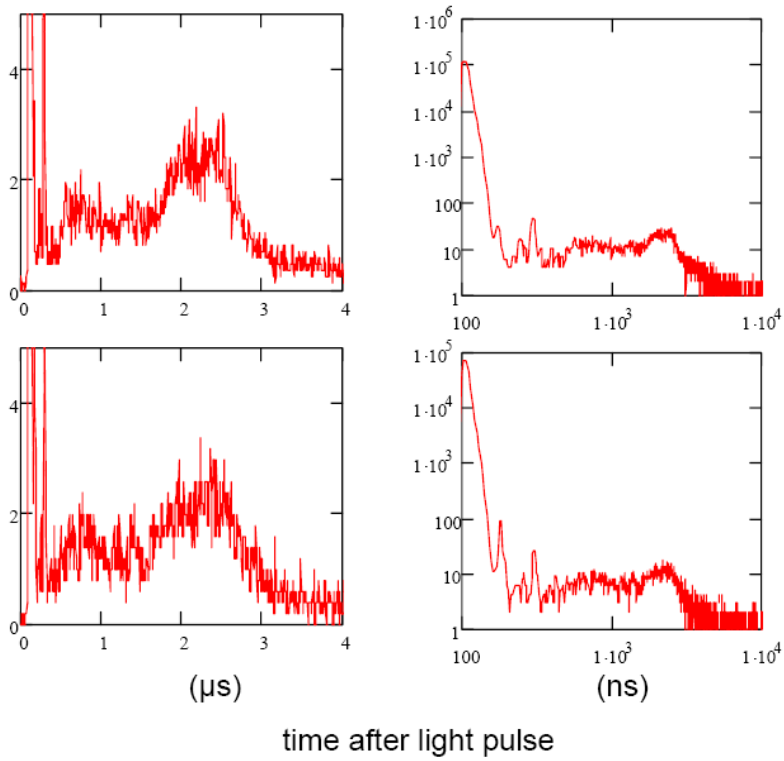

Fig.13: afterpulse time distribution, before and after the experiment under the same conditions (U_{PM} = 1720 V, T = 297 K). In between, the tube was stored for 12 hours in a dense He atmosphere at 8 K. Except for the axes (lin/log), the figs. on the left and the right are the same. In between the two measurements, the PM was exposed to helium gas at T = 8 K. There is no evidence for helium poisoning.

Fig.14: entire test assembly, ready to be inserted into the dewar. Shown are the test container at the bottom, the ¼” G10 supporting rods, the corrugated, flexible tube, and the radiation baffles. At the upper end there is the top flange that closes the well volume of the dewar. Above the top flange there is the feed-through box, and the pumping manifold.

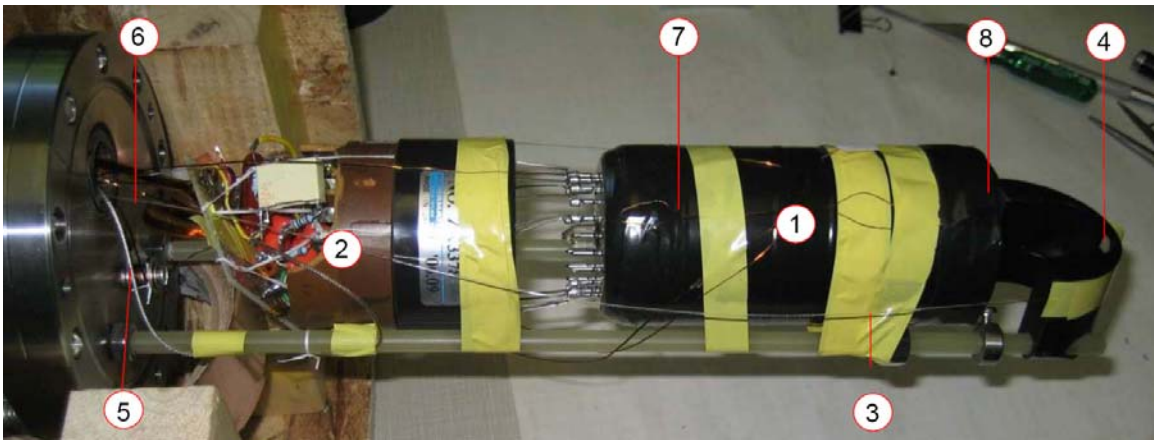

Fig.15: PM under test (1) with the test container removed. On the left is the Conflat flange without the copper seal. Also shown are the cold part of the base circuit (2), the optical fiber (3), the light splitter (4), the stainless steel coax signal cable (5), and the location of the temperature sensors (6-8).

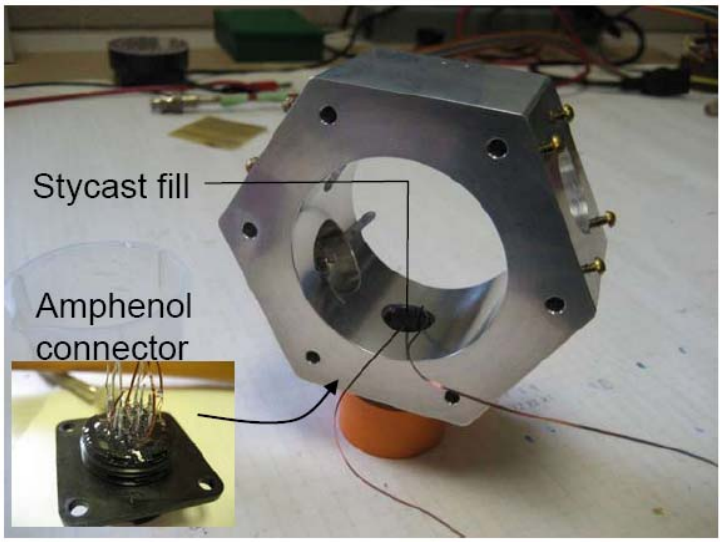

Fig.16: feed-through box with vacuum seals under construction. The Amphenol connectors are inserted from the outside and backfilled with Stycast epoxy.

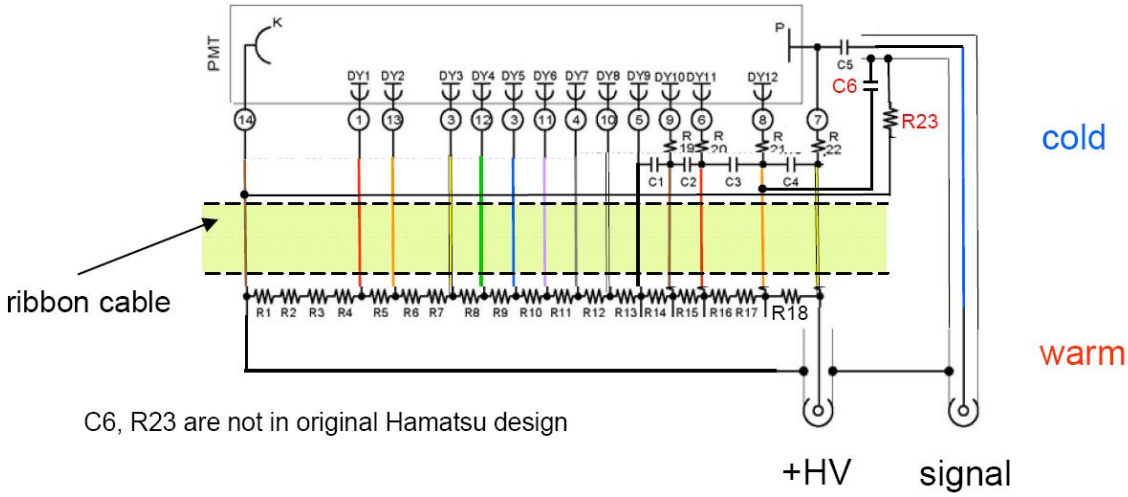

R1 – R18, R22, R23:	100kΩ	(Newark 74C0161)
R19 – R21, R23:	50Ω	(Newark 94C2108)
C1 – C4:	1nF, 600V	(Newark 15F2700)
C5, C6: 2.2nF,	2kV	(Newark 36K2459)

Fig.17: base circuit as suggested by Hamatsu. The added C6 and R23 provide current return close to the anode, and grounding of the shield near the tube. The components actually used (all tested for cryogenic performance) are listed. The ribbon cable is shown in fig.18.

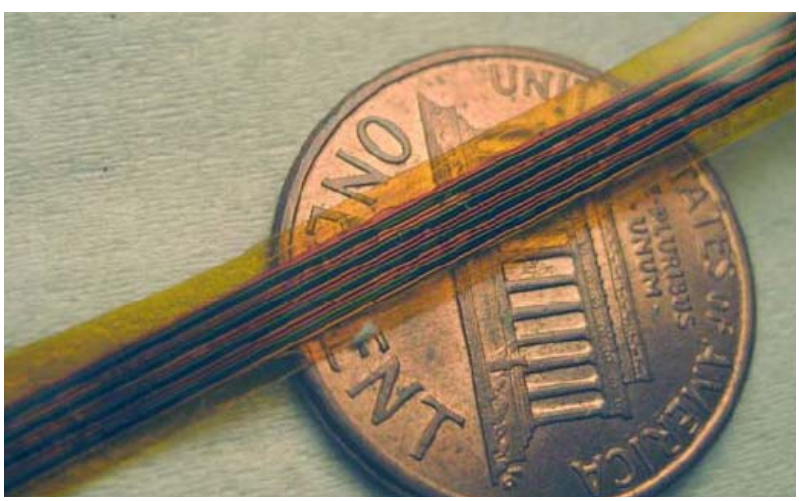

Fig.18: 16-strand ribbon cable, made from 36AWG (0.005” diameter) phosphor-bronze wires, embedded in transformer lacquer, sandwiched between Kapton foils. The cable holds 2000 V between the two outermost wires.

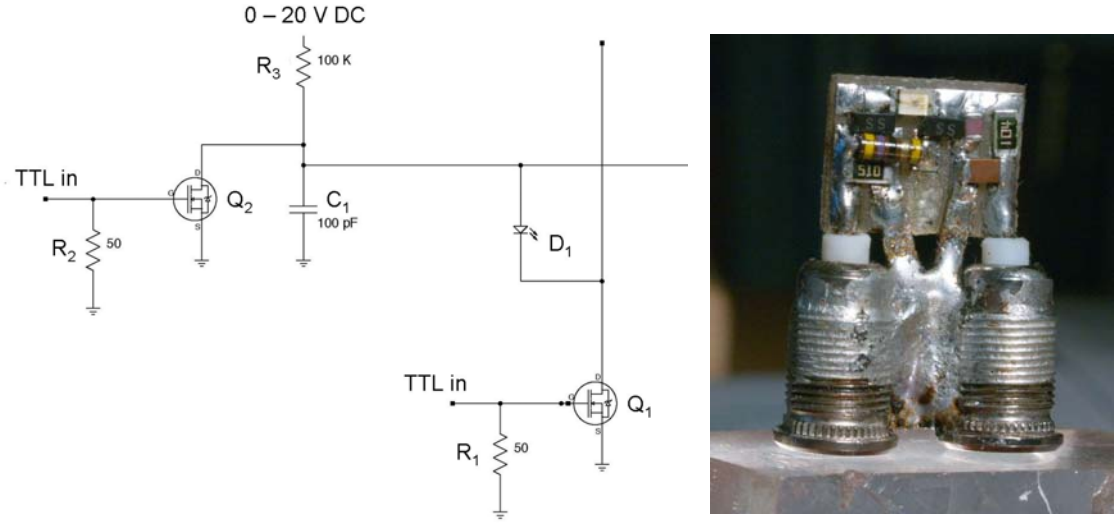

Fig.19: LED driver circuit. Switching Q1 allows the charge in C1 to flow through the LED (D1). The delayed closing of Q2 cuts off the exponential tail. The resulting light pulse is 10 – 15 ns wide. The amplitude may be varied by changing the DC supply voltage to C1. The physical layout is shown on the right (the two barrels are Lemo connectors, the LED is the white rectangle at the top).

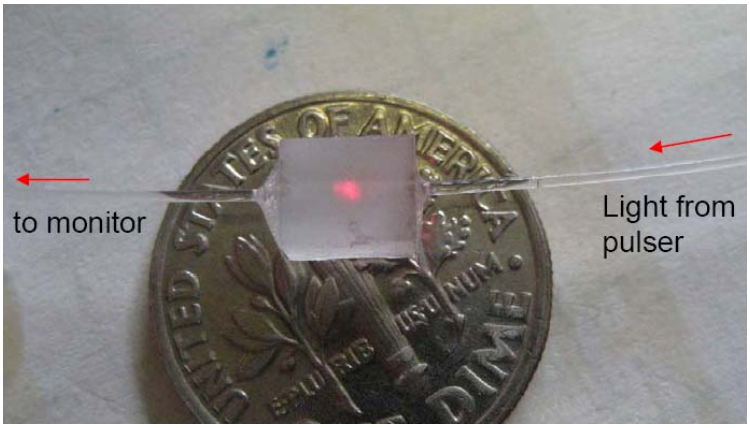

Fig.20: light splitter, positioned 3.5 cm in front of photocathode. The splitting is demonstrated by shining a laser pointer into the fiber.

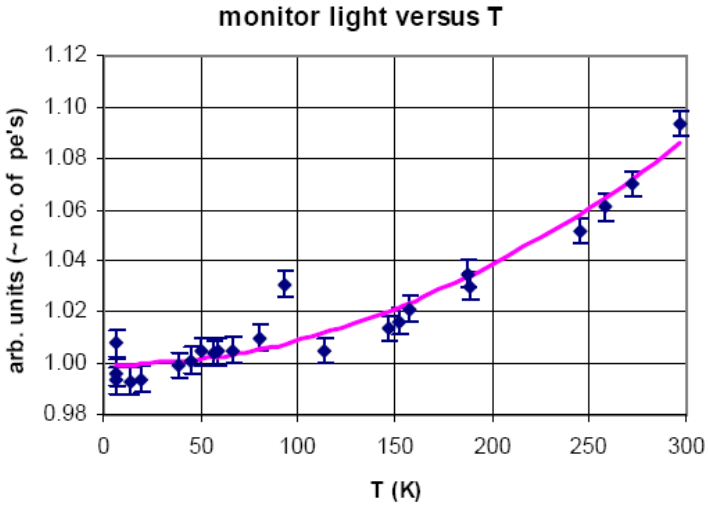

Fig.21: monitor light as a function of temperature, all other conditions being the same. The reason for the 10% drop is a temperature dependent change of the splitting fraction.

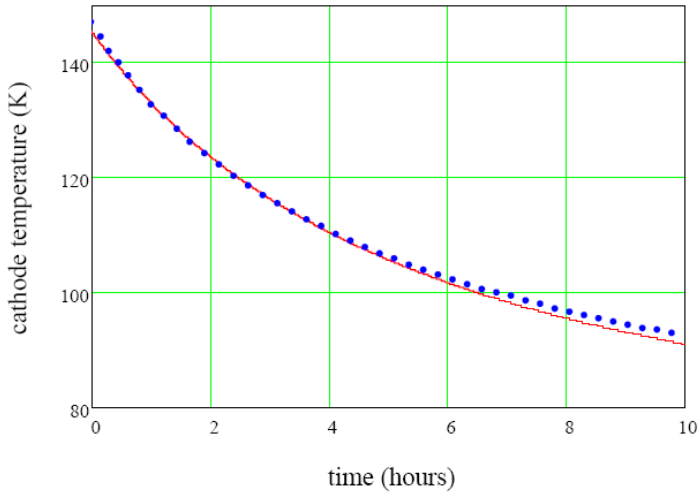

Fig.22: cooling by radiation. At $t = 0$, the test container was submersed in ℓN_2. The measured cathode temperature as a function of time (blue dots) is compared with a simulation (red line), using an emittance of 0.5 for both, the inside of the container wall and the surface of the photomultiplier.